Low noise 874 GHz receivers for the international submillimetre airborne radiometer (ISMAR)

N.B. When citing this work, cite the original published paper.

(article starts on next page)

Low noise 874 GHz receivers for the International Submillimetre Airborne Radiometer (ISMAR)

A. Hammar,[1,2,a)] P. Sobis,[1,2] V. Drakinskiy,[2] A. Emrich,[1] N. Wadefalk,[3] J. Schleeh,[3] and J. Stake[2]

[1]*Omnisys Instruments AB, August Barks Gata 6B, SE-421 32 Västra Frölunda, Sweden*
[2]*Terahertz and Millimetre Wave Laboratory, Department of Microtechnology and Nanoscience–MC2, Chalmers University of Technology, SE-412 96 Gothenburg, Sweden*
[3]*Low Noise Factory AB, Nellickevägen 22, SE-412 63 Gothenburg, Sweden*

We report on the development of two 874 GHz receiver channels with orthogonal polarizations for the International Submillimetre Airborne Radiometer. A spline horn antenna and dielectric lens, a Schottky diode mixer circuit, and an intermediate frequency (IF) low noise amplifier circuit were integrated in the same metallic split block housing. This resulted in a receiver mean double sideband (DSB) noise temperature of 3300 K (minimum 2770 K, maximum 3400 K), achieved at an operation temperature of 40 °C and across a 10 GHz wide IF band. A minimum DSB noise temperature of 2260 K at 20 °C was measured without the lens. Three different dielectric lens materials were tested and compared with respect to the radiation pattern and noise temperature. All three lenses were compliant in terms of radiation pattern, but one of the materials led to a reduction in noise temperature of approximately 200 K compared to the others. The loss in this lens was estimated to be 0.42 dB. The local oscillator chains have a power consumption of 24 W and consist of custom-designed Schottky diode quadruplers (5% power efficiency in operation, 8%–9% peak), commercial heterostructure barrier varactor (HBV) triplers, and power amplifiers that are pumped by using a common dielectric resonator oscillator at 36.43 GHz. Measurements of the radiation pattern showed a symmetric main beam lobe with full width half maximum <5° and side lobe levels below −20 dB. Return loss of a prototype of the spline horn and lens was measured using a network analyzer and frequency extenders to 750–1100 GHz. Time-domain analysis of the reflection coefficients shows that the reflections are below −25 dB and are dominated by the external waveguide interface. © *2018 Author(s). All article content, except where otherwise noted, is licensed under a Creative Commons Attribution (CC BY) license (http://creativecommons.org/licenses/by/4.0/).* https://doi.org/10.1063/1.5017583

I. INTRODUCTION

Ice clouds in the upper troposphere are important for the hydrological cycle and have a big impact on radiative transfer processes, which act to both cool and warm the Earth's atmosphere.[1] Yet, there is a lack of measurement data on ice clouds, which can help to improve current weather and climate models. Satellite-borne instruments that operate at sub-mm wavelengths are particularly suitable to gather these data due to strong interaction with ice particles and the capability to produce long-term data sets. Currently, a number of satellite missions utilize sub-mm radiometers to monitor the atmosphere.[2–4] However, none of these are specialized for retrievals of ice clouds. The Ice Cloud Imager (ICI) is a new satellite-borne instrument that will address this issue.[5] Planned for launch after 2020, this satellite will carry a total of 11 receiver channels that cover 183–664 GHz.

As a precursor for ICI, the International SubMillimetre Airborne Radiometer (ISMAR) instrument is currently being developed to test retrieval algorithms, calibration/validation schemes, etc.[6,7] ISMAR is installed onboard the FAAM BAe-146 Atmospheric Research Aircraft which is operated by the

UK Met Office. Similar to ICI, ISMAR has a total of seven receivers covering 118–664 GHz which have now been complemented by two new receivers operating at 874 GHz based on subharmonic Schottky diode mixers. The receivers of ISMAR are distributed in a cluster around the 118 GHz channel (see Fig. 1), and the mutually aligned beams from the antennas/lenses illuminate a flat rotating reflector that is mounted at an angle. This enables the beams to sweep over the atmospheric scene and into two temperature-controlled calibration loads.

Although receiver noise temperature typically increases with frequency, the new channels at 874 GHz are well suited for the detection of thin clouds, which consist of relatively small particles with strong scattering at short wavelengths. To minimize the noise temperature, high performance devices based on the Schottky diode and high-electron-mobility transistor (HEMT) technology were used for the front-ends. These key components were integrated with a spline horn antenna and dielectric lens in a single aluminum front-end split block. This minimized losses and helped to achieve the state-of-the-art noise performance for subharmonic mixer receivers (see Table I). Furthermore, the subharmonic mixers were designed for relatively low local oscillator (LO) power levels. Combined with newly developed high-efficiency Schottky diode
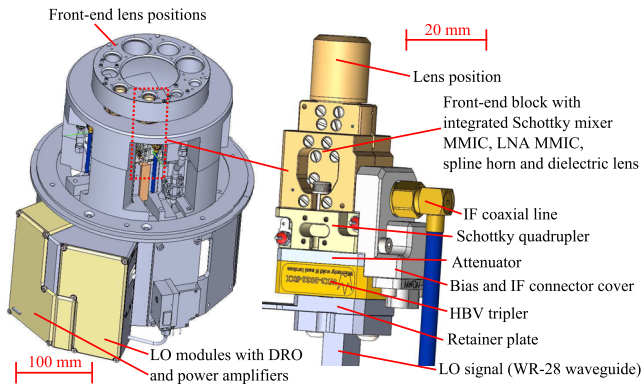
FIG. 1. CAD model showing the fixture for the cluster of receivers of ISMAR which cover 118–874 GHz. LO sources are mounted on the outer side of the cartridge ring structure that surrounds the front-ends that are connected via waveguides and coaxial lines. Only the two 874 GHz receivers are installed in the picture.

TABLE I. Comparison of DSB noise temperatures for receivers operating at room temperature. The acronyms SHM, FM, and SD used here denote the subharmonic mixer, fundamental mixer, and Schottky diode, respectively.

Frequency (GHz)	Receiver DSB noise temperature (K)	Type
1080	4000	SHM, GaAs SD[8]
874 (LO)	2260[a]	This work
874	4000[b]	SHM GaAs SD[9,10]
865.8	2330[b]/2500[c]	FM, GaAs SD[11]
850	2560	Amplifier, InP HEMT[12]
590	1100	SHM, GaAs SD[13]
557	2000	SHM, GaAs SD[14]
540	1070	SHM, GaAs SD[15]

[a]Measured at an operating temperature of 20 °C and with the lens removed.
[b]Extracted mixer noise.
[c]Value obtained by adding a noise contribution equivalent to the minimum (42 K) of the integrated IF LNA used in this work. It was also assumed that the mixer and the LNA have minimum noise at the same frequency and that the transmission between the two is lossless.

frequency multipliers, an overall high power efficiency was obtained for the front-ends.

In summary, this paper presents the development of two complete 874 GHz flight receivers (including the horn/lens antenna, front-ends, LO systems, and back-end) for ISMAR. The design and detailed characterization of the front-ends with the integrated horn/lens antenna, Schottky-diode mixer, intermediate frequency (IF) low noise amplifier (LNA), and corresponding LO systems are presented.

II. REQUIREMENTS AND IMPLEMENTATION

Two identical receivers with orthogonal polarizations at 874.4 GHz are needed for ISMAR. To achieve high enough spatial resolution, the radiation pattern of each receiver must have a main lobe full width half maximum (FWHM) smaller than 5° across a radio frequency (RF) bandwidth of 850–900 GHz. In addition, the receivers are required to have a maximum cross-polar level at least 20 dB below the maximum of the co-polar pattern and an RF port return loss less than −15 dB.

In the semi-external environment onboard the airplane, dielectric windows in front of the receivers are required to protect the front-end electronics. With an expected temperature of 40 ± 1 °C (controlled), the double sideband (DSB) noise temperature of the receivers must be less than 4000 K across an RF band of 874.4 ± 5.0 GHz. Both receivers are required to share a common LO source that uses less than 35 W during operation. The resulting IF bandwidth must be at least 3.5-8.5 GHz. The system as a whole is required to survive a temperature span of 10–50 °C. The LO-units of both 874 GHz receivers are to be mounted on the outer ring that surrounds the front-ends. A total mass of 2 kg for the complete 874 GHz dual polarization receivers is allowed on the air-borne platform.

III. DESIGN

A. Overview

The 874 GHz receivers of ISMAR are based on GaAs membrane Schottky diode mixers that are integrated with spline horn antennas and IF LNA monolithic microwave integrated circuits (MMICs) in a common gold-plated aluminum split block (Fig. 2). A single dielectric resonator oscillator (DRO) (Atlantic Microwave, model EDRO-1000 Series) at 36.433 GHz is used as a fundamental source for the LO chains that consist of power amplifiers (Spacek Labs, model SP384-25-29, coaxial to waveguide), heterostructure barrier varactor (HBV) frequency triplers (Wasa Millimeter Wave, model WX3-864#05), and custom-designed Schottky frequency quadruplers. For protection and reducing LO system standing waves, isolators (JQL Electronic, model JIWR28-28-5-36K4) with a maximum insertion loss of 0.6 dB were used. Two units housing the DRO, power amplifiers, and biasing circuitry as well as a total power back-end were built. Figure 3 shows all parts of the ISMAR 874 GHz receivers.

B. Lens and spline horn antenna

The gold-plated WR-1.2 rectangular waveguide (305 μm × 152 μm) used at the RF input to the mixer has typical insertion and flange losses of 0.15 dB/mm[16] and 1 dB, respectively. By integrating the spline horn antenna into the same metallic split block as the front-end mixer circuit, the RF waveguide flange interfaces could be eliminated and waveguide transmission losses reduced.
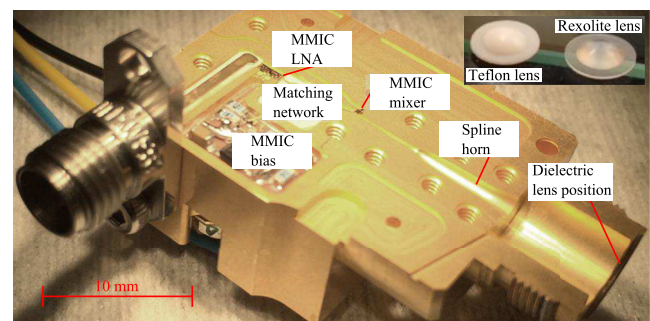

FIG. 2. Split block half showing the position of the dielectric lens, the spline horn, and the Schottky diode mixer MMIC with the corresponding bias circuit as well as LNA MMIC—all integrated in the same package.
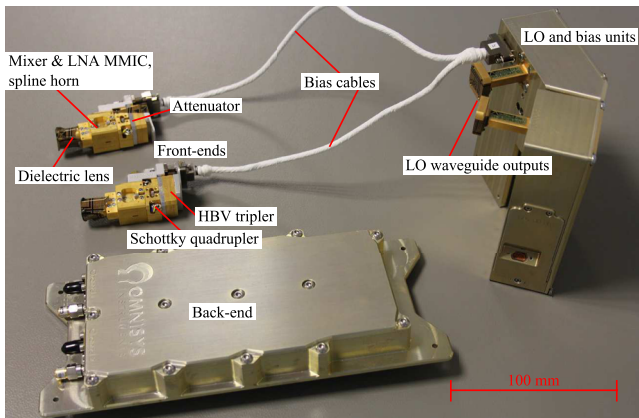
FIG. 3. Photo showing the manufactured flight hardware for the ISMAR 874 GHz channels.

The design of the horn antenna achieved a coupling to the fundamental Gaussian beam mode >98% across the RF band.[17] A least square fit between the simulated radiation pattern and an ideal Gaussian beam showed that the ISMAR horn has a beam waist of $\omega_0 = 0.45$ μm.

The horns were formed in the mixer split blocks using high-precision numerical milling.[18] Although the integrated horn topology has the advantage of decreased receiver noise temperature, a misalignment between the two block halves can have a negative impact on the system performance. A tolerance study was therefore performed to investigate the effects of lateral displacement between the two block halves. The far field was calculated using finite elements (Ansoft HFSS) at 874 GHz with the two block halves shifted in steps between 0 and 10 μm. The results show that the FWHM of the beam broadens less than $0.004°/\mu$m, whereas the peak of the cross-polar component in the $45°$ plane had an increase of 1.7 dB/μm. With a typical simulated cross-polar level of −28 dB, it was concluded that a lateral misalignment between the block halves less than 5 μm was required.

Three different dielectric lens materials (Rexolite 1422, Teflon, and Topas 5013L-10) were tested and compared to investigate the effect on the receiver noise temperature and radiation pattern. Although Topas was *a priori* expected to have the smallest losses (see Table II), it was still deemed instructive compared with the complexity of machining the different materials. Numerical milling was used to define the shape of the spherical dome of the lenses. A radial tool that worked in circles around the symmetry axis of the lens was used to obtain a surface with Ra < 3 μm. Teflon proved to be somewhat softer and therefore more difficult to machine

than Rexolite and Topas, although satisfactory results were obtained for all three materials. For each material, a set of lenses with different radii of curvature (five sets, ranging from 4.6 to 5.4 mm) were made so that the lens resulting in the smallest FWHM could be picked. In the prototyping phase, the distance between the horn aperture and the flat backside of the lens could be adjusted by using a stack of shims. This was exploited to optimize the lens position for a minimized FWHM. A detailed description of the lens design can be found in the study of Karandikar *et al.*[17]

C. Mixer and IF amplifier

The 874-GHz subharmonic Schottky diode mixer design is based on a broadband 600 GHz mixer prototype that was delivered in 2014 to the Max Planck Institute for Solar System Research (MPS) as part of the development of the front-end receiver for the Submillimetre Wave Instrument (SWI) onboard the ESA JUpiter ICy moons Explorer (JUICE) mission. The 600 GHz receiver front-end module had an integrated cryogenic IF LNA InP HEMT MMIC and reached an optimum receiver DSB noise temperature of 1100 K. This was measured at room temperature with approximately 1.5 mW of LO power (20% relative LO bandwidth). At 120 K operation temperature, the DSB noise temperature dropped to 900 K.

Both the 874 GHz and 600 GHz MMIC mixers were made from the same batch at Chalmers and were based on a 3 μm thick GaAs membrane (Fig. 4). These were optimized for 0.3 μm² anodes using a 64 nm active layer with a doping concentration of $3 \cdot 10^7$ cm⁻³ on a 1.5 μm thick highly doped buffer layer. The diode devices were measured on-wafer and had a DC series resistance and an ideality factor of approximately 22 Ω and 1.18, respectively. Neglecting resistive losses in the embedding circuit, a minimum single sideband conversion loss of 7 dB at the −2 dBm LO power level was achieved at 874 GHz using harmonic balance simulations. This translates into an optimum LO power of approximately 1.5 mW for the 3D electromagnetic model of the complete MMIC package, including realistic losses implemented as a 50% reduction in conductivity in metallic walls and conductors. Details about the device processing can be found in the study of Zhao *et al.*[21]

A room temperature IF LNA MMIC circuit based on an InP HEMT from the Low Noise Factory (model LNF_LNR4-14B) with a custom biasing and filter board was integrated
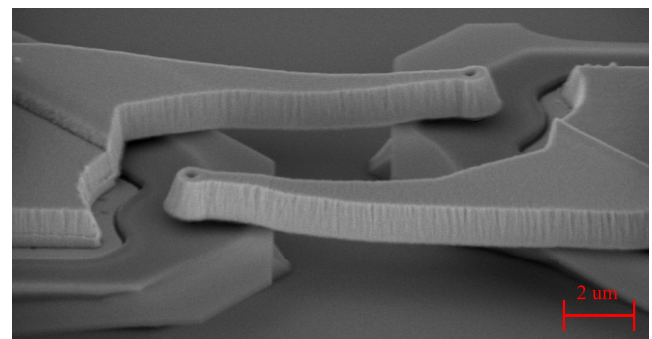
TABLE II. Relative permittivity, loss tangent, radius of curvature, and horn aperture to lens backside distance of the plano-convex lenses.

Material	ϵ_r (−)	$\tan \delta$ (−)	R (mm)	d (mm)
Rexolite[19]	2.50	0.001-0.005	5.2	6.6
Teflon[20]	2.08	$13.1 \cdot 10^{-4}$	4.7	6.4
Topas 5013L-10[a]	2.34	$2.54 \cdot 10^{-4}$	5.0	6.5

[a]Topas gave the lowest losses (see Sec. IV) and was therefore used for the delivered hardware.

FIG. 4. SEM image of anti-parallel Schottky diodes with ~0.3 μm² large anodes.
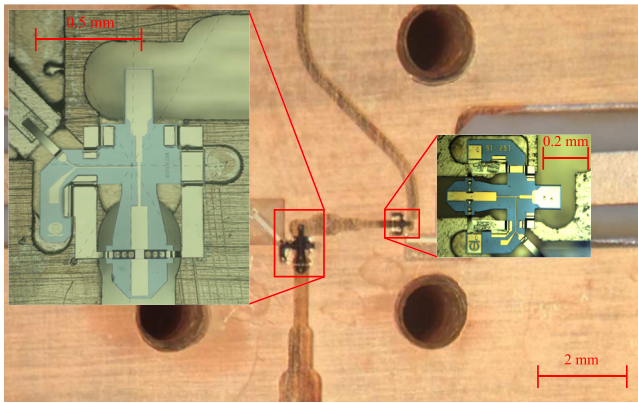
FIG. 5. Inside of the quadrupler split block with Schottky doubler MMIC circuits highlighted.

inside the mixer block in order to minimize losses and standing waves.[22] This LNA has a noise performance optimum in the range 4-14 GHz (50 Ω system) and a typical gain of 37 dB. The expected maximum noise contribution at the 3.5-8.5 GHz band from the LNA is estimated to be 60 K at 50 °C. Due to impedance differences between the mixer and the LNA, the system exhibits a small shift in the frequency response compared to a separately packaged LNA.

D. LO multiplier chain

The high power HBV frequency tripler is based on a single chip that is mounted inside a compact metallic waveguide block with a WR-22 input and WR-10 output. Coupling between the waveguides and the HBV chip is established by using open-ended waveguide probes that in turn connect to impedance matching networks that are realized using microstrips. A key feature of the HBV is the voltage dependent capacitance, which has its maximum at zero voltage.[23] This in turn results in a component that can operate without biasing. A conversion efficiency of 23% with a maximum input power of 800 mW over a 15% 3-dB bandwidth has been reported for these components.[24] The device processing is described in detail in the study of Malko *et al.*[24]

Two cascaded Schottky diode varactor MMIC doublers were used to realize the quadrupler units (see Fig. 5), which deliver a 440 GHz LO signal for the subharmonic mixers. Both doubler MMICs were passivated using a 60 nm thick layer of plasma-enhanced chemical vapor deposition (PECVD) SiN$_x$. From simulations that include realistic losses, the doublers exhibit peak power efficiencies of 35% and 25% for the first and second stage, respectively. Integrated in the system at the fixed LO output frequency of 437.2 GHz, the quadrupler power efficiency was typically 5%. The LO output powers of the two multiplier chains were tuned to 2.5-3.5 mW, leaving about 0.5 mW margin above the mixer optimum LO power.

IV. RESULTS

A. Spline horn and lens

The beam produced by the spline horn and dielectric lens was measured using a setup with a rotational scanner that
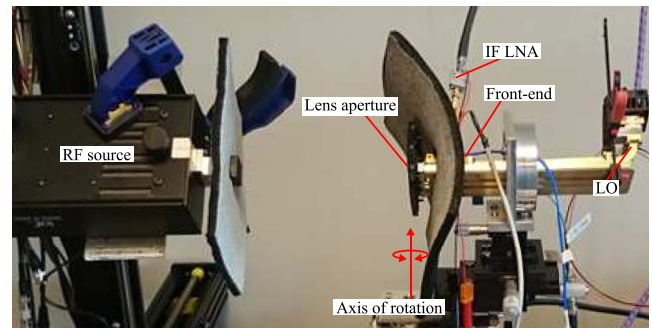
recorded the far field radiation pattern in the E, H, and 45° planes. As shown in Fig. 6, the receiver chain was placed on the rotational scanner while facing an RF source.

A x9 frequency multiplier (Virginia Diodes, model WR9.0SGX) with an additional frequency tripler and diagonal feed horn (WR-1.2) at the output was pumped by a signal at ~10.8 GHz. The ninth harmonic from the output tripler was utilized to obtain the 874 GHz RF signal, while the third harmonic at ~291 GHz was well below the cutoff frequency of both horns used in the setup. Using this high-order harmonic made the resulting RF signal relatively weak, which limited the dynamic range of the measurement. Two yttrium iron garnet (YIG) oscillator synthesizers with a number of cascaded solid-state multipliers were used to generate signals for the RF source and the receiver LO. No phase reference signal was used in the configuration, and, hence, only power could be measured. The IF signal from the receiver was amplified using an LNA and mixed down to match the bandwidth of the Omnisys digital FFT spectrometer with 10 000 channels that was used as the back-end.

The distance between the horn aperture and the backside of the lens was tuned using a stack of shims of different thicknesses in order to find the best position that resulted in the narrowest beam. Satisfactory results were obtained for all three lens materials (cf. Table II), but since Topas has the lowest losses, it was used for the flight modules. Radiation patterns in the E, H, and 45° planes for the Topas lens at 868.7 and 880.0 GHz are shown in Fig. 7. Despite the weak source
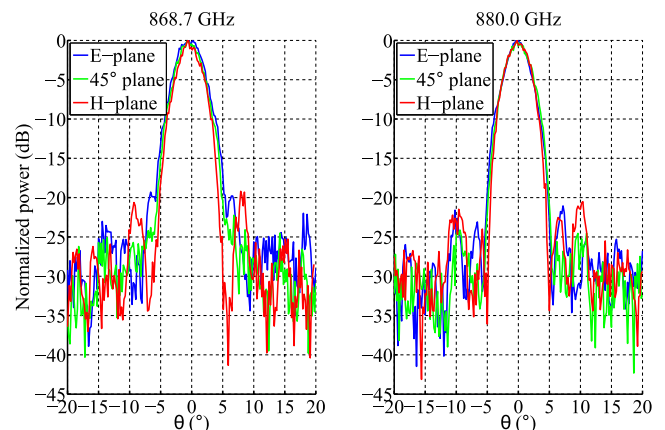

FIG. 6. Setup for measuring the radiation pattern of the spline horn and lens.

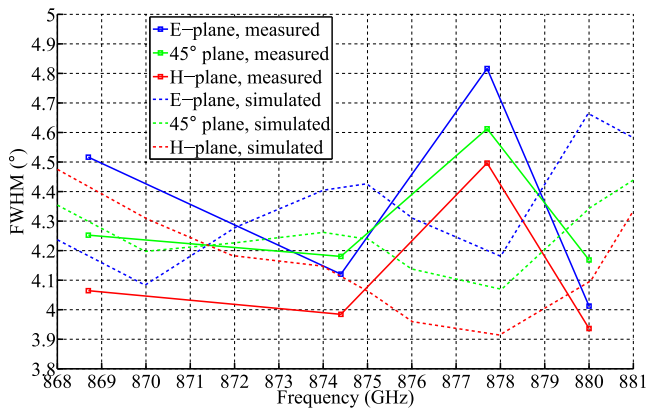FIG. 7. Normalized far field radiation patterns from the spline horn and Topas lens in three φ planes.

FIG. 8. Comparison between the measured and simulated FWHM of the spline horn and Topas lens.

signal, it was possible to resolve side lobes below −20 dB with excellent repeatability. Measurements were performed at 868.7, 874.4, 877.7, and 880 GHz. The FWHM at these frequencies are compared to simulations in Fig. 8. As can be seen, the FWHM is well below 5° across the entire RF band.

Since the noise floor started to appear below −25 dB in the co-polar measurements, it was clear that measurements of the cross-polar radiation pattern that had a simulated peak between −30 and −24 dB would be challenging. Only noise could be seen when measuring cross polarization in the 45° plane, which indicates low cross-polar levels. As a best effort, the alignment between the two front-end block halves was measured to ensure that the displacement was less than 5 μm (cf. Sec. III).

A prototype split block with a spline horn and a Topas lens was connected to a VDI 750–1100 GHz vector network analyzer (VNA) extender to measure the return loss of the antenna. The results show that the return loss varies between −25 and −20 dB across the entire RF band, i.e., well below the required −15 dB. An analysis in the time domain was made to distinguish between the amount of reflections at various reference planes. As can be seen in Fig. 9, two different lens
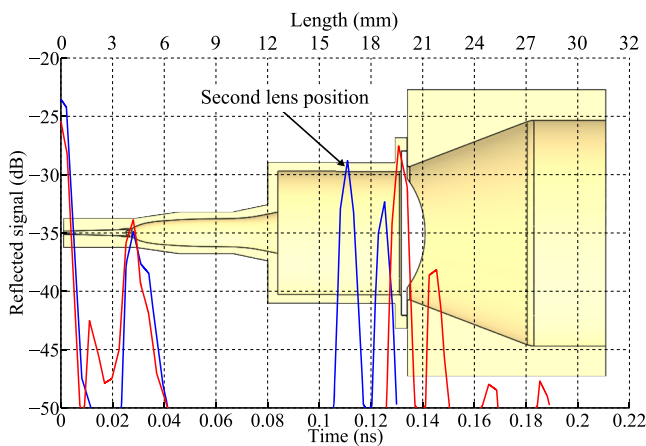

FIG. 9. Time-domain measurements of the spline horn and Topas lens. Two measurements (corresponding to the blue and red lines) were made, where the distance between the horn aperture and the lens was varied. NB: The length scale at the top is with reference to the physical size of the horn/lens plotted in the figure. The second roundtrip after reflections is thus neglected in this scale that differs by a factor of two compared to the time scale at the bottom.

positions were tested to clearly identify the peaks that correspond to the two faces of the lens. It is also clear that reflections from the waveguide interface dominate both over the transition from rectangular waveguide to the circular spline horn and the backside of the lens.

B. LO multiplier chain

Five different HBV tripler units were tested with peak output powers above 200 mW at 108 GHz. For the final LO multiplier configuration, two HBV triplers with approximately 120 mW of output power were selected and a custom-made WR-10 waveguide attenuator (~3 dB) was inserted between the HBV tripler and the quadrupler, which was optimized for 60 mW of input power.

Figure 10 shows the output power and power efficiency of one of the Schottky quadruplers when directly connected to the HBV tripler. A typical power efficiency of approximately 5% was measured for the integrated quadrupler modules when matching the output power to the optimum LO pumping power of the mixer. During the hardware development, a maximum efficiency of 7.4% was obtained for a prototype quadrupler that produced an output power of 4.2 mW. Losses in the WR-3.4-WR-10 waveguide taper and WR-10 waveguide (both 1 in. long) that were used between the quadrupler output and the power meter (VDI Erickson PM5) were estimated to be 0.7 dB. Standing waves in the setup also add to the measurement uncertainties. Taking these effects into account, the highest power efficiency was estimated to be 8%–9%.

C. Receiver noise temperature

To accurately measure the noise temperature of the receivers, a tri-reflector Y-factor setup with two calibration loads was used; see Fig. 11. Two off-axis reflectors were used to focus the beam from the horn and steer it toward a flat reflector, which was directly mounted on a step motor to enable switching between the loads. The focal lengths of the first two reflectors were chosen so that the output beam waist would be located between the switching reflector and the aperture of the calibration loads. Moreover, by placing the beam waist of the horn at the focal point of the first reflector and separating the reflectors by a distance equal to the sum of their focal
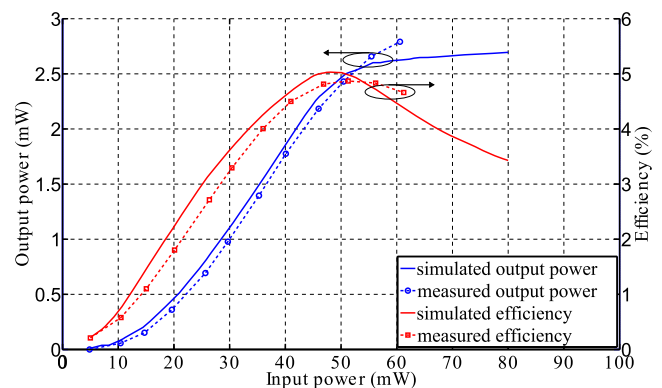

FIG. 10. Simulated and measured output power and power efficiency of the Schottky diode quadrupler as a function of input power.
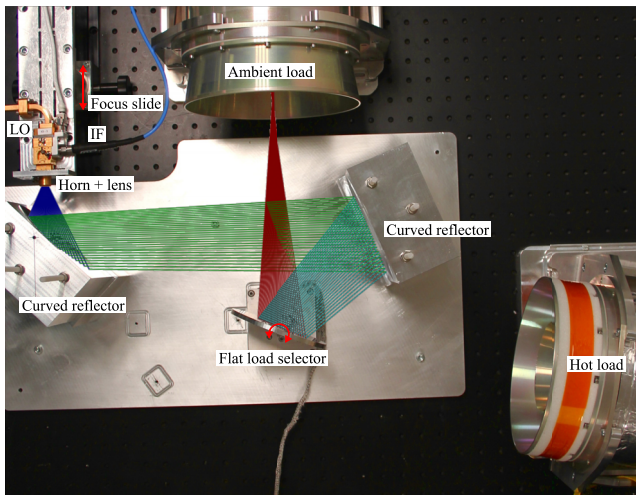
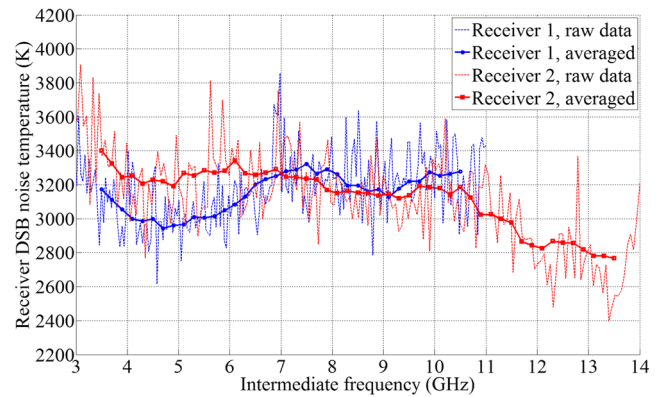FIG. 11. Y-factor setup used for noise temperature measurements.

FIG. 12. Receiver DSB noise temperature as a function of intermediate frequency for the 874 GHz flight receivers for ISMAR. The data are corrected for losses in the setup. An averaging window of width 1 GHz was used. The temperature of the front-ends was regulated to 40 °C.

lengths, the location of the output waist is ensured not to shift as the frequency changes.[20] The total distance between the horn aperture and the loads is 1.1 m.

Broadband (31–950 GHz) calibration loads originally developed for the Atacama Large Millimeter/submillimeter Array (ALMA)[25] were used as hot and ambient loads. The former was regulated to $T_{hot} = 355$ K, whereas the temperature of the latter was monitored at room temperature ($T_{amb} = 294$ K) during the data acquisition. The mixer IF signal was amplified using an LNA and subsequently mixed down using an IQ mixer to match the 2.5 GHz bandwidth of the FFT spectrometer used as the back-end. To mimic the operating conditions on the ISMAR platform, the temperature of the front-end was actively regulated to 40 °C using resistive heaters.

Taking the ratio of the total power delivered to the back-end when observing the hot and ambient loads gives the Y-factor,

$$Y(\nu) = \frac{T_{rec,DSB}(\nu) + T_{hot}}{T_{rec,DSB}(\nu) + T_{amb}}, \quad (1)$$

from which the DSB noise temperature can be obtained

$$T_{rec,DSB}(\nu) = \frac{T_{hot} - Y(\nu)T_{amb}}{Y(\nu) - 1}. \quad (2)$$

Signal losses from the hot load to the lens aperture act to decrease the effective radiometric temperature experienced by the receiver and should therefore be taken into account to more accurately estimate the receiver noise temperature. To assess spill over effects, the ISMAR horn was approximated with an ideal Gaussian beam ($\omega_0 = 0.45$). Simulations in GRASP 10.0.1 show that the total spillover was down to a numerical noise level at 874 GHz. With an over-sized reflector and load apertures, the alignment tolerances of the reflectors became loose and spill over effects could therefore be ignored altogether.

Ohmic loss in each reflector leads to decreased reflectance, which is given by $\eta_{cond} = 1 - 4\sqrt{\pi\epsilon_0\nu/\sigma_{cond}}$, where the conductivity of aluminum at room temperature σ_{cond} was taken to be $1.6 \cdot 10^7$ S/m. Hence, the total reflectance in the three mirrors becomes $\eta_{cond} = 0.9852$. Absorption in the air was

calculated using the *g*aspl routine in Matlab. With measurements performed at room temperature (294 K) and a relative humidity of 50%, the average transmission power efficiency in the RF band becomes $\eta_{abs} = 0.9772$. The reduction in the power throughput due to scattering losses was approximated by using Ruze's equation $\eta_{ruze} = \exp(-(4\pi\sigma_{ruze}/\lambda)^2)$, where σ_{ruze} is the RMS surface roughness. Although the surface figures of the reflectors were never measured, in-house experiences show that reflectors of this kind typically have an RMS roughness less than 1 μm. Assuming $\sigma_{ruze} = 1$ μm, the scattering loss becomes 0.9986.

Figure 12 shows the DSB noise temperature for the two delivered flight receivers. Unfortunately, one of the receivers was only characterized within the specified IF bandwidth required for ISMAR. An average setup loss of 144 K is estimated across the IF band for the ISMAR receiver. Regardless of whether setup losses are taken into account or not, the receiver has a noise temperature well below the required 4000 K across the entire IF band. The mean double sideband noise temperature is 3300 K, whereas the minimum and maximum are 2770 and 3400 K, respectively. Moreover, losses in the dielectric lens were estimated to be 0.42 ± 0.2 dB. Correcting for the losses due to the lens, the receiver has a DSB noise temperature of 2470 and 3100 K. At 20 °C (i.e., with no temperature regulation), a minimum receiver noise temperature of 2260 K was measured at 861 GHz for a receiver with the lens removed.

V. CONCLUSION

The two 874 GHz receiver channels for ISMAR have been built and tested with a mean noise DSB noise temperature of 3300 K (minimum 2770 K, maximum 3400 K) across an IF bandwidth of 10 GHz. Correcting for losses in the dielectric lens, this figure becomes 3000 K (minimum 2470 K, maximum 3100 K). At 20 °C, a minimum noise temperature of 2260 K was measured at 861 GHz for a receiver without lens. To the best knowledge of the authors, this is the lowest reported noise temperature for a room temperature receiver operating at these frequencies. This was achieved by integrating state-of-the-art mixer/IF LNA MMICs and the smooth-walled spline horn in a

common metallic split block and by using a low-loss lens material (Topas 5013L-10). The Schottky diode quadruplers for the LO signal generation had a measured 5% power efficiency in operation and 8%–9% peak efficiency. Good power efficiency and a compact/lightweight solution with an integrated spline horn and lens make this type of integrated receiver suitable not only for an air-borne instrument like ISMAR but also for space-borne missions.

The measured far field patterns from the lens and horn are compliant with the FWHM $<5°$ requirement and in good agreement with simulations. Time-domain measurements using a 750–1100 GHz frequency extender showed that reflections from the waveguide interface between the horn and the extender dominate over reflections from the rectangular to circular waveguide taper in the horn and the backside of the lens. This clearly emphasizes the value of integrating the feed horn into the mixer split block. Moreover, the small tolerances made possible by the numerical milling machine that was used to define the spline horn makes this concept scalable to frequencies well above 1 THz. However, full-wave simulations of misaligned split blocks showed that the far field main lobe broadens by $0.004°/\mu m$ and that the cross-polar component increases by 1.7 dB$/\mu m$.

ACKNOWLEDGMENTS

[1] S. A. Buehler, C. Jiménez, K. F. Evans, P. Eriksson, B. Rydberg, A. J. Heymsfield, C. J. Stubenrauch, U. Lohmann, C. Emde, V. O. John, T. R. Sreerekha, and C. P. Davis, Q. J. R. Metereol. Soc. **133**, 109 (2007).

[2] P. Eriksson, M. Ekström, B. Rydberg, and D. P. Murtagh, Atmos. Chem. Phys. **7**, 471 (2007).

[3] J.-L. Li, D. E. Waliser, J. H. Jiang, D. L. Wu, W. Read, J. W. Waters, A. M. Tompkins, L. J. Donner, J.-D. Chern, W.-K. Tao, R. Atlas, Y. Gu, K. N. Liou, A. Del Genio, M. Khairoutdinov, and A. Gettelman, Geophys. Res. Lett. **32**, L18710, https://doi.org/10.1029/2005GL023788 (2005).

[4] Y. Hong and G. Liu, J. Clim. **28**, 3880 (2015).

[5] M. Bergadá, M. Labriola, R. González, M. A. Palacios, D. Marote, A. Andrés, J. L. García, D. S. Pascuala, L. Ordóñez, M. Rodríguez, M. T. Ortín, V. Esteso, J. Martínez, and U. Klein, in *2016 14th Specialist Meeting on Microwave Radiometry and Remote Sensing of the Environment (MicroRad)* (IEEE, 2016), pp. 27–31.

[6] S. Fox, C. Lee, B. Moyna, M. Philipp, I. Rule, S. Rogers, R. King, M. Oldfield, S. Rea, M. Henry, H. Wang, and R. C. Harlow, Atmos. Meas. Tech. **10**, 477 (2017).

[7] M. Brath, S. Fox, P. Eriksson, R. C. Harlow, M. Burgdorf, and S. A. Buehler, Atmos. Meas. Tech. **11**, 611 (2018).

[8] E. Schlecht, J. V. Siles, C. Lee, R. Lin, B. Thomas, G. Chattopadhyay, and I. Mehdi, IEEE Trans. Terahertz Sci. Technol. **4**, 661 (2014).

[9] E. W. Bryerton and J. L. Hesler, in *2017 42nd International Conference on Infrared, Millimeter, and Terahertz Waves (IRMMW-THz)* (IEEE, 2017), pp. 1–2.

[10] E. W. Bryerton, J. L. Hesler, S. A. Retzloff, and T. W. Crowe, in *2016 IEEE International Geoscience and Remote Sensing Symposium (IGARSS)* (IEEE, 2016), pp. 5553–5555.

[11] B. Thomas, A. Maestrini, J. Gill, C. Lee, R. Lin, I. Mehdi, and P. de Maagt, IEEE Trans. Microwave Theory Tech. **58**, 1917 (2010).

[12] K. M. K. H. Leong, X. Mei, W. H. Yoshida, A. Zamora, J. G. Padilla, B. S. Gorospe, K. Nguyen, and W. R. Deal, IEEE Trans. Terahertz Sci. Technol. **7**, 466 (2017).

[13] K. Jacob, A. Murk, H. Kim, P. Sobis, A. Emrich, V. Drakinskiy, J. Stake, A. Maestrini, J. Treuttel, F. Tamazouzt, B. Thomas, M. Philipp, and P. Hartogh, in 36th ESA Antenna Workshop, ESTEC, Noordwijk, The Netherlands, 2015.

[14] P. F. X. Neumaier, H. Richter, J. Stake, H. Zhao, A. Y. Tang, V. Drakinskiy, P. Sobis, A. Emrich, A. Hulsmann, T. K. Johansen, T. Bryllert, J. Hanning, V. Krozer, and H. W. Hubers, IEEE Trans. Terahertz Sci. Technol. **4**, 469 (2014).

[15] J. Treuttel, L. Gatilova, A. Maestrini, D. Moro-Melgar, F. Yang, F. Tamazouzt, T. Vacelet, Y. Jin, A. Cavanna, J. Matéos, A. Féret, C. Chaumont, and C. Goldstein, IEEE Trans. Terahertz Sci. Technol. **6**, 148 (2016).

[16] See http://vadiodes.com/VDI/pdf/waveguidechart200908.pdf for "Virginia diodes, inc. waveguide band designations;" accessed 2017-01-07.

[17] Y. Karandikar, A. Hammar, P. Sobis, P. Forsberg, A. Emrich, and J. Stake, in *2015 9th European Conference on Antennas and Propagation (EuCAP)* (IEEE, 2015), pp. 1–5.

[18] A. Hammar, D. Nyberg, Y. Karandikar, P. Sobis, O. Tropp, P. Forsberg, S. McCallion, A. Emrich, and J. Stake, in *2016 IEEE International Symposium on Antennas and Propagation (APSURSI)* (IEEE, 2016), pp. 1341–1342.

[19] R. H. Giles, A. J. Gatesman, and J. Waldman, Int. J. Infrared Millimeter Waves **11**, 1299 (1990).

[20] P. Goldsmith, *Quasioptical Systems: Gaussian Beam Quasioptical Propagation and Applications*, IEEE Press Series on RF and Microwave Technology (Wiley, 1998).

[21] H. Zhao, V. Drakinskiy, P. Sobis, J. Hanning, T. Bryllert, A.-Y. Tang, and J. Stake, in *2012 International Conference on Indium Phosphide and Related Materials* (IEEE, 2012), pp. 102–105.

[22] P. J. Sobis, N. Wadefalk, A. Emrich, and J. Stake, IEEE Microwave Wireless Compon. Lett. **22**, 366 (2012).

[23] J. Stake, A. Malko, T. Bryllert, and J. Vukusic, Proc. IEEE **105**, 1008 (2017).

[24] A. Malko, T. Bryllert, J. Vukusic, and J. Stake, in *2012 International Conference on Indium Phosphide and Related Materials* (IEEE, 2012), pp. 92–94.

[25] P. Yagoubov, A. Murk, R. Wylde, G. Bell, and G. H. Tan, in *2011 International Conference on Infrared, Millimeter, and Terahertz Waves* (IEEE, 2011), pp. 1–2.